

UPPER-BOUND SOLUTIONS FOR BEARING CAPACITY OF FOUNDATIONS

By Abdul-Hamid Soubra¹

ABSTRACT: The static and seismic bearing capacity problem of shallow strip footings is investigated. Two kinematically admissible failure mechanisms M1 and M2 are considered in the framework of the upper-bound method of the limit analysis theory. The M1 mechanism is symmetrical, and it permits the calculation of the bearing capacity in the case of no-seismic loading. It is composed of a triangular active wedge under the footing and two radial shear zones composed of a sequence of rigid triangles. The M2 mechanism is nonsymmetrical and is composed of a single radial shear zone. This mechanism permits the calculation of the bearing capacity in the presence of seismic loading. Quasi-static representation of earthquake effects using the seismic coefficient concept is adopted. The solutions obtained are rigorous upper-bound ones in the framework of the limit analysis theory. The numerical results of the static and seismic bearing capacity factors are presented in the form of design charts for practical use in geotechnical engineering. These results are compared with results of other authors.

INTRODUCTION

The bearing capacity of strip footings in no-seismic areas has been extensively studied by several investigators [Terzaghi (1943), Caquot and Kérisel (1953), Meyerhof (1963), Vesic (1973), and Chen (1975) among others]. However, very few attempts have been made to study the effect of an earthquake on the bearing capacity of foundations. The few studies available in the literature describing the seismic effect on the bearing capacity concern the work of Meyerhof (1951) and Shinohara et al. (1960). Both approaches are pseudostatic: horizontal and vertical accelerations are applied to the center of gravity of the structure and the problem is reduced to a static case of bearing capacity with inclined eccentric loads. However, in these solutions, the inertia of the soil mass is not included. Sarma and Iossifelis (1990) and Richards et al. (1993) suggested more rigorous approaches for calculating the seismic bearing capacity of strip footings in seismic areas by considering the inertia forces on all parts of the soil-structure system (soil and foundation). The theoretical approaches they used are based on the limit-equilibrium method. It is well known that this method gives an approximate solution of the failure load and that the solution cannot be said to be an upper- or a lower-bound one with respect to the exact solution. Recently, Dormieux and Pecker (1995) and Soubra (1997) used the upper-bound method of the limit analysis theory and developed upper-bound solutions of the seismic bearing capacity factors. These solutions are rigorous upper-bound ones with respect to the exact solutions for an associated flow rule Coulomb material.

In this paper, both the static and seismic bearing capacity problems are investigated by the upper-bound method of the limit analysis theory using respectively symmetrical and nonsymmetrical failure mechanisms. These mechanisms allow the slip surface to develop more freely in comparison with the available mechanisms given by Chen (1975) and Soubra (1997); hence, they lead to smaller upper-bound solutions of the bearing capacity problem.

UPPER AND LOWER BOUND THEOREMS OF LIMIT ANALYSIS

The upper-bound theorem, which assumes a perfectly plastic soil model with an associated flow rule, states that the internal

power dissipated by any kinematically admissible velocity field can be equated to the power dissipated by the external loads and so enables a strict upper-bound on the true limit load to be deduced. A kinematically admissible velocity field is one that satisfies compatibility, the flow rule, and the velocity boundary conditions. To provide solutions that are useful in practice, the upper-bound theorem is often used in tandem with the lower-bound theorem. The latter also assumes a perfectly plastic soil model with an associated flow rule and states that any statically admissible stress field (which satisfies equilibrium and the stress boundary conditions and nowhere violates the yield criterion) will furnish a lower-bound estimate of the true limit load. By using these two theorems, the exact limit load can often be bracketed with an accuracy that is sufficient for design purposes.

In this paper, only the upper-bound theorem of limit analysis is applied to the static and seismic bearing capacity problem using kinematically admissible velocity fields. It should be noted here, that the upper-bound theorem gives an unsafe estimate of the ultimate bearing capacity. The aim of this work is to improve the best available upper-bound solutions given by Chen (1975) in the symmetrical failure mechanism and by Soubra (1997) in the nonsymmetrical mechanism.

THEORETICAL ANALYSIS OF STATIC AND SEISMIC BEARING CAPACITY PROBLEM

A soil-foundation system with translational movement is assumed. Two distinct translational failure mechanisms, referred to as the M1 and M2 mechanisms, are utilized in the analysis. In the following investigation, the terms "mechanism" and "velocity field" will be used interchangeably. Note that the velocity fields used are composed of rigid blocks that move with constant velocities. Since no general plastic deformation of the soil mass is permitted to occur, the power is dissipated solely at the interfaces between adjacent blocks, which constitute velocity discontinuities.

The soil is homogeneous and isotropic. It is assumed to be an associated flow rule Coulomb material obeying Hill's maximal work principle. The consequence of applying the normality condition to a frictional soil with its angle of internal friction equal to ϕ will be a necessary occurrence of a volume expansion with $\Psi = \phi$ during the plastic flow. However, frictional soils are found experimentally to dilate at increments considerably less than those predicted by the normality condition, that is, $\Psi < \phi$. Hence, real soils do not obey the associative flow rule. Furthermore, it is well known that a non-associative material cannot be stronger than the associative one. On the other hand, it should be mentioned that in translational failure mechanisms, the energy balance approach for evaluation of the limit load is always equivalent to the equilibrium of forces approach, because the energy balance equa-

¹Maître de Conférences, Ecole Nationale Supérieure des Arts et Industries de Strasbourg, 24, Bd de la victoire, 67084 Strasbourg cedex, France.

Note. Discussion open until June 1, 1999. To extend the closing date one month, a written request must be filed with the ASCE Manager of Journals. The manuscript for this paper was submitted for review and possible publication on October 2, 1997. This paper is part of the *Journal of Geotechnical and Geoenvironmental Engineering*, Vol. 125, No. 1, January, 1999. ©ASCE, ISSN 1090-0241/99/0001-0059-0068/\$8.00 + \$.50 per page. Paper No. 16729.

tion can be interpreted as an expression of the virtual rate of work principle. This observation has often been made (Davis 1968; Mroz and Drescher 1969; Michalowski 1989; Salençon 1990; De Buhan and Salençon 1993; Drescher and Detournay 1993). The equivalence of the two approaches plays a key role in the derivations of the limit loads for nonassociative materials. Recent theoretical considerations made on translational failure mechanisms (Drescher and Detournay 1993; Michalowski and Shi 1995, 1996) allow one to conclude that for a nonassociative material, the limit load can be obtained by the use of the flow rule associated with a new yield condition in which c and ϕ are replaced by c^* and ϕ^* as follows:

$$\tan \phi^* = \frac{\cos \Psi \sin \phi}{1 - \sin \Psi \sin \phi} \quad (1)$$

$$c^* = \frac{\cos \Psi \cos \phi}{1 - \sin \Psi \sin \phi} c \quad (2)$$

Hence, the results presented in the present paper can be used for nonassociative material provided the internal friction angle ϕ and the cohesion c are replaced with ϕ^* and c^* calculated from (1) and (2), respectively.

Failure Mechanisms

M1 Mechanism

The M1 mechanism is shown in Fig. 1. This mechanism is symmetrical, and it permits the calculation of the bearing ca-

capacity in the case of no-seismic loading. The wedge ABC is translating vertically as a rigid body with the same initial downward velocity as the footing. The downward movement of the footing and wedge is accommodated by the lateral movement of the adjacent soil as indicated by the two radial shear zones. The angles θ , α_i , and β_i ($i = 1, \dots, n$) are as yet unspecified. Since the movement is symmetrical about the footing, it is only necessary to consider the movement on the right-hand side of Fig. 1.

The radial shear zone BCD is composed of n triangular rigid blocks. As shown in Fig. 2(a), all the triangles move as rigid bodies in directions that make an angle ϕ with the discontinuity lines d_i ($i = 1, \dots, n$). The velocity of each triangle is determined by the condition that the relative velocity between the triangles in contact must have the direction that makes an angle ϕ to the contact surface. The velocity hodographs are shown in Fig. 2(b). The velocities so determined constitute a kinematically admissible velocity field.

As shown in Fig. 3, the external forces contributing to the incremental external work consist of the foundation load, the weight of the soil mass, and the surcharge q on the foundation level. The incremental external work for the different external forces can be easily obtained; the calculations are presented in Appendix I.

Energy is dissipated at the discontinuity surfaces d_i ($i = 1, \dots, n$) between the material at rest and the material in motion and at the discontinuity surfaces l_i ($i = 1, \dots, n$) within the radial shear zone. The incremental energy dissipation per unit

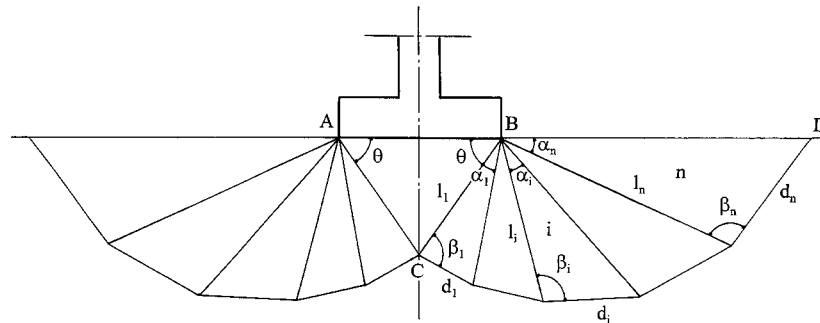


FIG. 1. Failure Mechanism M1 for Static Bearing Capacity Analysis

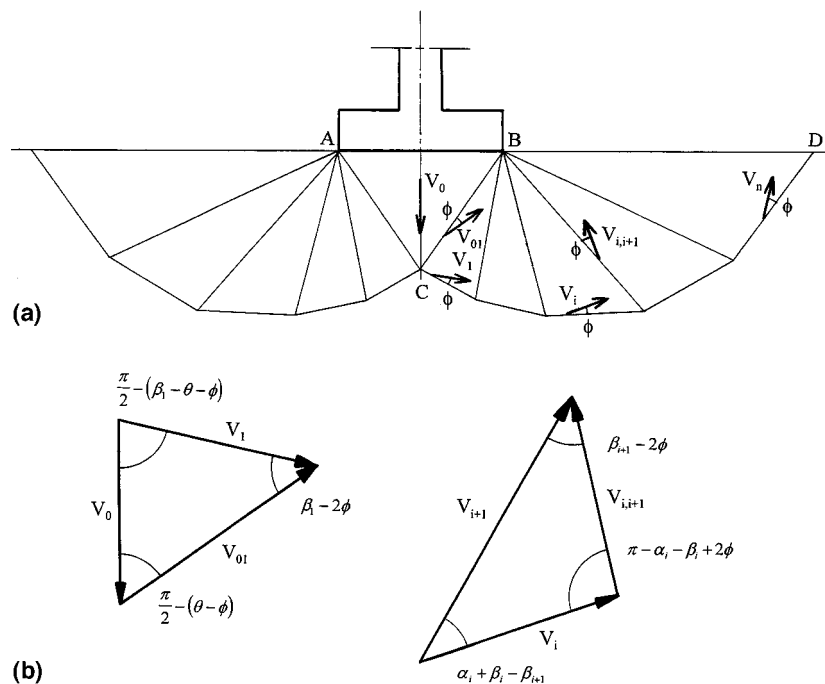


FIG. 2. (a) Velocity Field of M1 Mechanism; (b) Velocity Hodographs

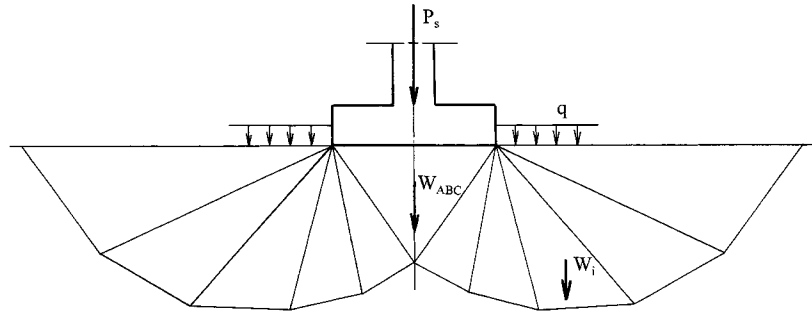


FIG. 3. Free-Body Diagram for M1 Failure Mechanism

length along a velocity discontinuity or a narrow transition zone can be expressed as

$$\Delta D_L = c \Delta V \cos \phi \quad (3)$$

where ΔV = incremental displacement or velocity that makes an angle ϕ with the velocity discontinuity according to the associated flow rule of perfect plasticity; and c = cohesion parameter. Calculations of the incremental internal energy dissipation along the lines of velocity discontinuities are given in Appendix I.

Equating the total rate at which work is done by the force on the foundation, the soil weight in motion, and the surcharge loading [(26) in Appendix I] to the total rate of energy dissipation along the lines of velocity discontinuities [(33) in Appendix I], it is found, after some simplifications, that an upper bound on the bearing capacity of the soil is

$$q_{cs} = \frac{P_s}{B_0} = \gamma \frac{B_0}{2} N_{\gamma s}(\theta, \alpha_i, \beta_i) + q N_{qs}(\theta, \alpha_i, \beta_i) + c N_{cs}(\theta, \alpha_i, \beta_i) \quad (4)$$

in which the static bearing capacity factors $N_{\gamma s}(\theta, \alpha_i, \beta_i)$, $N_{qs}(\theta, \alpha_i, \beta_i)$, and $N_{cs}(\theta, \alpha_i, \beta_i)$ can be expressed in terms of the $(2n + 1)$ as yet unspecified angles $(\theta, \alpha_i, \beta_i)$. They are given as follows:

$$N_{\gamma s} = -(f_1 + f_2) \quad (5)$$

$$N_{qs} = -f_3 \quad (6)$$

$$N_{cs} = 2(f_4 + f_5 + f_6) \quad (7)$$

The ultimate static bearing capacity of the foundation is obtained by minimization of q_{cs} [(4)] with regard to the mechanism's parameters. However, in practice, the minimum values of the three factors $N_{\gamma s}(\theta, \alpha_i, \beta_i)$, $N_{qs}(\theta, \alpha_i, \beta_i)$, and $N_{cs}(\theta, \alpha_i, \beta_i)$ are determined independently of each other, and therefore their use errs on the safe side (see Static Bearing Capacity Factors in the fourth section).

M2 Mechanism

The M2 mechanism is shown in Fig. 4. This mechanism is nonsymmetrical, and it permits the calculation of the bearing capacity in the presence of seismic loading. As is well known, an earthquake has two possible effects on a soil-foundation system. One is to increase the driving forces, and the other is to decrease the shearing resistance of the soil. In this paper, only the reduction of the bearing capacity due to the increase in driving forces is investigated under seismic loading conditions. The shear strength of the soil is assumed to remain unaffected by the seismic loading. On the other hand, the earthquake acceleration for both the soil and the structure is assumed to be the same: Only the horizontal seismic coefficient K_h is considered, the vertical seismic coefficient often being disregarded. Finally, the earthquake load on the structure is represented by the base shear load acting at the foundation

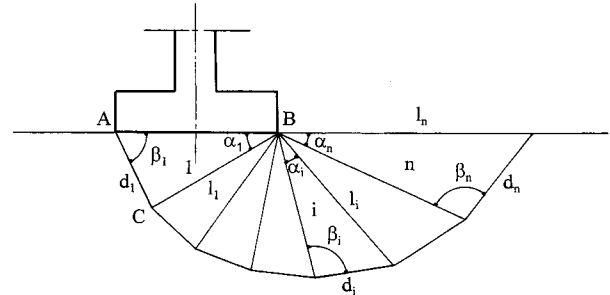
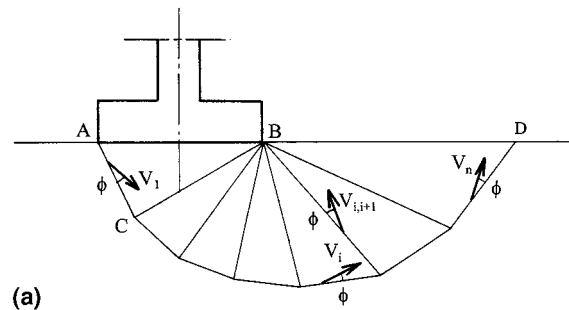
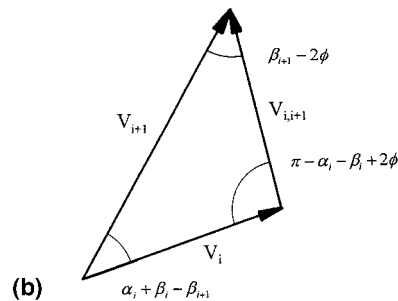


FIG. 4. Failure Mechanism M2 for Seismic Bearing Capacity Analysis



(a)



(b)

FIG. 5. (a) Velocity Field of M2 Mechanism; (b) Velocity Hodo-graph

level and an eccentricity for the vertical foundation load. The moment due to the seismic load on the structure is not considered. Only the base shear load will be taken into account.

Except for the triangular area directly below the base of the footing, the M2 nonsymmetrical mechanism is similar to the right-hand side of the M1 mechanism. Wedge ABC is translating as a rigid body with a downward velocity V_i inclined at an angle ϕ to the discontinuity line AC (Fig. 5). The foundation is assumed to move with the same velocity as wedge ABC (i.e., V_i). The rest of the mechanism is similar in form to the right-hand side of the M1 mechanism.

As shown in Fig. 6, the external forces contributing to the incremental external work consist of the force acting on the footing, the weight of soil in motion, the surcharge loading, and the different inertia forces. These inertia forces concern

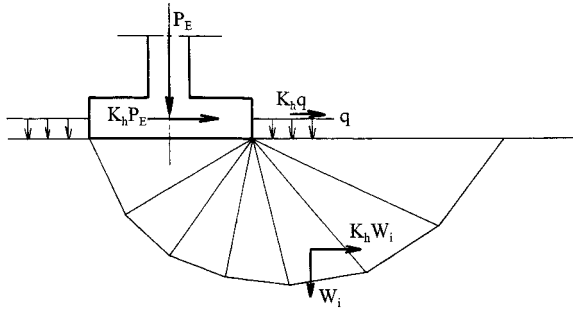


FIG. 6. Free-Body Diagram for M2 Failure Mechanism

the base shear load, the inertia forces of the soil in motion, and the surcharge loading. Energy is dissipated along the lines l_i ($i = 1, \dots, n - 1$) and d_i ($i = 1, \dots, n$). Calculations of the incremental external work and the internal energy dissipation along the different velocity discontinuities are given in Appendix II.

Equating the total external rate of work [(44) in Appendix II] to the total internal rate of energy dissipation [(49) in Appendix II], it is found that the value of the upper bound on the bearing capacity is

$$q_{cE} = \frac{P_E}{B_0} = \gamma \frac{B_0}{2} N_{\gamma E}(\alpha_i, \beta_i) + q N_{qE}(\alpha_i, \beta_i) + c N_{cE}(\alpha_i, \beta_i) \quad (8)$$

in which the seismic bearing capacity factors $N_{\gamma E}(\alpha_i, \beta_i)$, $N_{qE}(\alpha_i, \beta_i)$, and $N_{cE}(\alpha_i, \beta_i)$ can be expressed in terms of the $(2n)$ as yet unspecified angles (α_i, β_i) . They are given as follows:

$$N_{\gamma E} = -\frac{1}{\sin(\beta_1 - \phi) + K_h \cos(\beta_1 - \phi)} (g_1 + K_h g_2) \quad (9)$$

$$N_{qE} = -\frac{1}{\sin(\beta_1 - \phi) + K_h \cos(\beta_1 - \phi)} (g_3 + K_h g_4) \quad (10)$$

$$N_{cE} = \frac{1}{\sin(\beta_1 - \phi) + K_h \cos(\beta_1 - \phi)} (g_5 + g_6) \quad (11)$$

From these equations, it is clear that only the $N_{\gamma E}$ factor includes the soil inertia. The N_{qE} factor includes the inertia of the foundation load and the surcharge loading; however, the N_{cE} factor only includes the inertia of the foundation load and thus corresponds to the case of a footing subject to an inclined load.

As in the static case, the minimum value of q_{cE} gives the ultimate seismic bearing capacity of the foundation. However, in practice, the minimum values of the three factors $N_{\gamma E}(\alpha_i, \beta_i)$, $N_{qE}(\alpha_i, \beta_i)$, and $N_{cE}(\alpha_i, \beta_i)$ are determined independently of each other, and therefore their use errs on the safe side.

NUMERICAL RESULTS

The most critical bearing capacity factors can be obtained by minimization of these factors [(5)–(7) and (9)–(11)] with regard to the mechanism's parameters. The minimization procedure can be performed using the optimization tool available in most spreadsheet software packages. In this paper, one uses the Solver optimization tool of Microsoft Excel. Two computer programs using the Visual Basic programming language that resides in Microsoft Excel have been written to define the static and seismic bearing capacity factors as function of the mechanism's parameters [(5)–(7) and (9)–(11)]. Initial values need to be assigned to the different angular parameters. The solver tool is then invoked to “minimize” the bearing capacity factor “by changing” the angular parameters, “subject to” the constraints $\{\theta + \sum_{i=1}^n \alpha_i = \pi$ (cf. Fig. 1) and $\alpha_i + \beta_i \geq \beta_{i+1}$ [cf. Fig. 2(b)] for the M1 mechanism and $\{\sum_{i=1}^n \alpha_i = \pi$ (cf.

Fig. 4) and $\alpha_i + \beta_i \geq \beta_{i+1}$ [cf. Fig. 5(b)] for the M2 mechanism. The method of minimization used is the general reduced gradient method. Additional information on Solver options and algorithms can be found in the Microsoft Excel Solver's help file and at the website www.frontsys.com.

In the following sections, we present and discuss in succession (1) the static bearing capacity factors $N_{\gamma S}$, N_{qS} , and N_{cS} given by both the M1 and M2 mechanisms; and (2) the seismic bearing capacity factors $N_{\gamma E}$, N_{qE} , and N_{cE} given by the M2 nonsymmetrical mechanism.

Static Bearing Capacity Factors

First, the results given by the M1 symmetrical mechanism will be presented and compared to those given by other existing solutions. Second, the results of the M2 nonsymmetrical mechanism for $K_h = 0$ will be presented and compared to those given by the M1 symmetrical mechanism. This permits us to estimate the difference between results when considering a nonsymmetrical mechanism for a centrally loaded footing.

Table 1 presents the $N_{\gamma S}$ factor obtained from the M1 mechanism for $\phi = 45^\circ$ and for various values of n (the number of the triangular rigid blocks). It can be observed that the upper-bound solution can be improved by increasing the number of rigid blocks. The reduction in the $N_{\gamma S}$ value decreases with the n -increase and attains 0.2% for $n = 14$. It should be mentioned that the same trend is also observed for the N_{qS} and N_{cS} factors.

Fig. 7 shows the critical slip surface obtained from the numerical minimization of the $N_{\gamma S}$ factor for $\phi = 45^\circ$ and for $n = 12$. It can be observed that the critical failure mechanism obtained by the computer program is composed of two radial shear zones sandwiched between an active triangular wedge under the footing and a Rankine passive wedge. It should be noted that the radial shear zones are not bounded by log-spiral slip surfaces as is the case of the Prandtl mechanism. Finally, note that all subsequent calculations are made for $n = 14$.

Table 2 presents the $N_{\gamma S}$, N_{qS} , and N_{cS} factors obtained from the computer program for ϕ ranging from 0 to 50° .

To check the effect of the superposition method, one calculates the ultimate load P_{direct} obtained by direct numerical minimization of P_S [(4)] and compares it to the one obtained by the superposition method $P_{\text{superposition}}$ using the $N_{\gamma S}$, N_{qS} , and N_{cS} factors. For $\phi = 30^\circ$, $c = 10$ kPa, $q = 10$ kPa, $B_0 = 1$ m, and $\gamma = 18$ kN/m³, one obtains $P_{\text{direct}} = 726.13$ kN/m and

TABLE 1. $N_{\gamma S}$ Value versus Number of Rigid Blocks n for $\phi = 45^\circ$ from M1 Symmetrical Mechanism

n (1)	$N_{\gamma S}$ (2)	Reduction (%) (3)
2	741.93	—
3	447.94	39.6
4	384.28	14.2
5	359.50	6.4
6	347.19	3.4
7	340.16	2.0
8	335.76	1.3
9	332.82	0.9
10	330.77	0.6
11	329.27	0.5
12	328.14	0.3
13	327.27	0.3
14	326.59	0.2

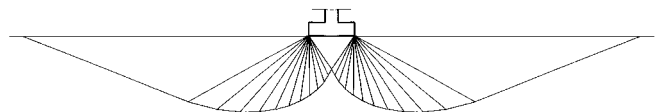


FIG. 7. Critical Slip Surface for $\phi = 45^\circ$ and $n = 12$

TABLE 2. $N_{\gamma S}$, N_{qS} , and N_{cS} Values from M1 Symmetrical Mechanism

ϕ (1)	$N_{\gamma S}$ (2)	N_{qS} (3)	N_{cS} (4)
0	—	1.00	5.15
1	—	1.09	5.38
2	—	1.20	5.64
3	—	1.31	5.91
4	—	1.43	6.19
5	—	1.57	6.50
6	—	1.72	6.82
7	—	1.88	7.17
8	—	2.06	7.54
9	—	2.26	7.93
10	—	2.47	8.36
11	—	2.71	8.81
12	—	2.98	9.30
13	—	3.27	9.82
14	1.62	3.59	10.39
15	1.95	3.95	10.99
16	2.32	4.34	11.65
17	2.75	4.78	12.36
18	3.25	5.27	13.13
19	3.82	5.81	13.96
20	4.49	6.41	14.86
21	5.26	7.08	15.85
22	6.15	7.84	16.92
23	7.19	8.68	18.09
24	8.40	9.62	19.37
25	9.81	10.69	20.77
26	11.46	11.88	22.32
27	13.39	13.23	24.01
28	15.67	14.76	25.88
29	18.35	16.49	27.95
30	21.51	18.46	30.24
31	25.26	20.70	32.79
32	29.71	23.26	35.62
33	35.02	26.19	38.79
34	41.37	29.56	42.34
35	49.00	33.44	46.33
36	58.21	37.93	50.82
37	69.35	43.13	55.91
38	82.91	49.19	61.68
39	99.48	56.27	68.25
40	119.84	64.58	75.77
41	144.99	74.36	84.40
42	176.23	85.95	94.35
43	215.27	99.73	105.87
44	264.39	116.20	119.29
45	326.59	135.99	134.99
46	405.97	159.91	153.46
47	508.04	189.00	175.31
48	640.42	224.59	201.32
49	813.64	268.44	232.49
50	1,042.48	322.88	270.09

$P_{\text{superposition}} = 680.58 \text{ kN/m}$, which indicates that the superposition effect errs on the safe side.

Comparison of Results with Existing Solutions

$N_{\gamma S}$ Factor. As is well known, there are a great many solutions for $N_{\gamma S}$ in the literature based on different methods and the differences among them are sometimes substantial. Because of the great sensibility of the $N_{\gamma S}$ factor to the friction angle, particularly for $\phi > 30^\circ$, the tendency today, in practice, is to use the values given by Caquot and Kérisel (1953), Meyerhof (1963) [cf. (12)], and Vesic (1973) [cf. (13)]

$$N_{\gamma S}(\text{Meyerhof}) = (N_{qS} - 1)\tan 1.4\phi \quad (12)$$

$$N_{\gamma S}(\text{Vesic}) = 2(N_{qS} + 1)\tan \phi \quad (13)$$

where N_{qS} is given as follows:

$$N_{qS} = \exp(\pi \tan \phi) \tan^2 \left(\frac{\pi}{4} + \frac{\phi}{2} \right) \quad (14)$$

The values given by Caquot and Kérisel and the expression suggested by Vesic are being increasingly used. Table 3 and Fig. 8 show the comparison with the aforementioned authors. The maximal difference between the present solution and that of Caquot and Kérisel is smaller than 10% for $\phi \leq 45^\circ$.

On the other hand, rigorous upper-bound solutions for an associated flow rule Coulomb material are proposed in the literature. Chen (1975) considered three symmetrical failure mechanisms referred to as Prandtl1, Prandtl2, and Prandtl3 and gave rigorous upper-bound solutions in the framework of the limit analysis theory. Prandtl1 is composed of a triangular active wedge under the footing, two radial log-spiral shear zones and two triangular passive wedges. Prandtl2 differs from Prandtl1 only in that an additional rigid body zone has been introduced. Finally, Prandtl3 resembles closely the Prandtl1 mechanism; however, each shear zone is now bounded by a circular arc. The upper-bound solutions given by the present M1 mechanism and those given by the three aforementioned mechanisms proposed by Chen are presented in Table 4. It is clear that the present upper-bound solutions are better than

TABLE 3. Comparison of Present $N_{\gamma S}$ Factor with that of Other Authors

ϕ (1)	Present solution (M1) (2)	Caquot and Kérisel (1953) (3)	Meyerhof (1963) (4)	Vesic (1973) (5)
20	4.49	4.97	2.87	5.39
25	9.81	10.4	6.77	10.88
30	27.51	21.8	15.67	22.4
35	49.0	48.0	37.15	48.03
40	119.84	113.0	93.69	109.41
45	326.59	297.0	262.74	271.76

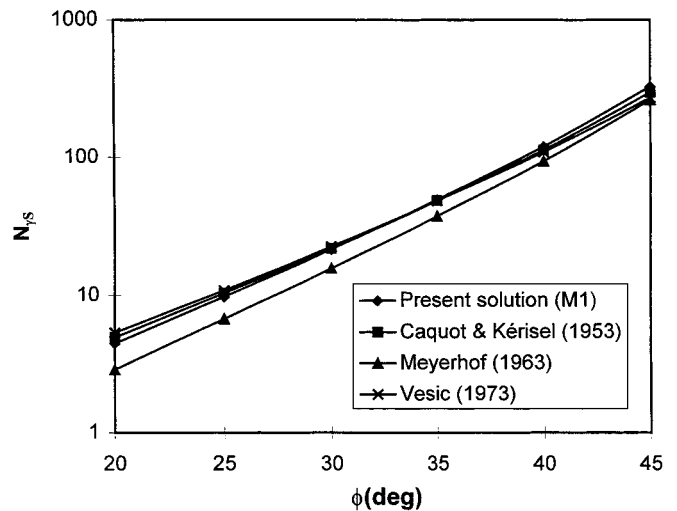


FIG. 8. Comparison of Present $N_{\gamma S}$ Factor with Results of Other Authors

TABLE 4. Comparison of Present $N_{\gamma S}$ Factor with Other Upper-Bound Solutions

ϕ (1)	Present solution (M1) (2)	Chen (1975)		
		Prandtl1 (3)	Prandtl2 (4)	Prandtl3 (5)
15	1.9	2.7	2.3	2.1
20	4.5	5.9	5.2	4.6
25	9.8	12.4	11.4	10.9
30	21.5	26.7	25.0	31.5
35	49.0	60.2	57.0	138.0
40	119.8	147.0	141.0	1,803.0

those of Chen (1975); the improvement attains 15% for $\phi = 40^\circ$.

N_{qs} and N_{cs} Factors. Based on the upper-bound method of the limit analysis theory, the bearing capacity factors obtained from Prandtl mechanism are given by (14) for N_{qs} and by (15) for N_{cs} [cf. Chen (1975)]

$$N_{cs} = (N_{qs} - 1)\cot \phi \quad (15)$$

It should be mentioned here that Chen (1975) has also shown that the bearing capacity factors N_{cs} and N_{qs} as given by (14) and (15) are also lower bounds and hence are the exact solutions in the framework of the limit analysis theory.

The comparison of the present factors with those given by (14) and (15) has shown that the present solutions are very close to the exact solutions; the error does not exceed 1.2%.

TABLE 5. $N_{\gamma s}$, N_{qs} , N_{cs} Values from M2 Nonsymmetrical Mechanism

ϕ (1)	$N_{\gamma s}$ (2)	N_{qs} (3)	N_{cs} (4)
0	—	1.00	5.15
1	0.03	1.09	5.38
2	0.07	1.20	5.64
3	0.11	1.31	5.91
4	0.17	1.43	6.19
5	0.25	1.57	6.50
6	0.33	1.72	6.82
7	0.43	1.88	7.17
8	0.55	2.06	7.54
9	0.69	2.26	7.93
10	0.85	2.47	8.36
11	1.03	2.71	8.81
12	1.24	2.98	9.30
13	1.49	3.27	9.82
14	1.77	3.59	10.39
15	2.10	3.95	11.00
16	2.47	4.34	11.65
17	2.91	4.78	12.36
18	3.41	5.26	13.13
19	3.99	5.81	13.96
20	4.67	6.41	14.87
21	5.45	7.08	15.85
22	6.35	7.84	16.92
23	7.40	8.68	18.09
24	8.63	9.62	19.38
25	10.06	10.69	20.78
26	11.73	11.88	22.32
27	13.68	13.23	24.02
28	15.98	14.76	25.89
29	18.69	16.49	27.96
30	21.88	18.46	30.25
31	25.67	20.70	32.80
32	30.16	23.25	35.63
33	35.52	26.18	38.80
34	41.93	29.55	42.36
35	49.62	33.43	46.35
36	58.90	37.91	50.84
37	70.13	43.11	55.93
38	83.78	49.17	61.71
39	100.47	56.24	68.28
40	120.96	64.55	75.80
41	146.27	74.33	84.44
42	177.70	85.91	94.40
43	216.97	99.68	105.94
44	266.35	116.13	119.37
45	328.88	135.91	135.09
46	408.65	159.81	153.58
47	511.22	188.86	175.45
48	644.19	224.42	201.50
49	818.14	268.22	232.70
50	1,047.90	322.59	270.36

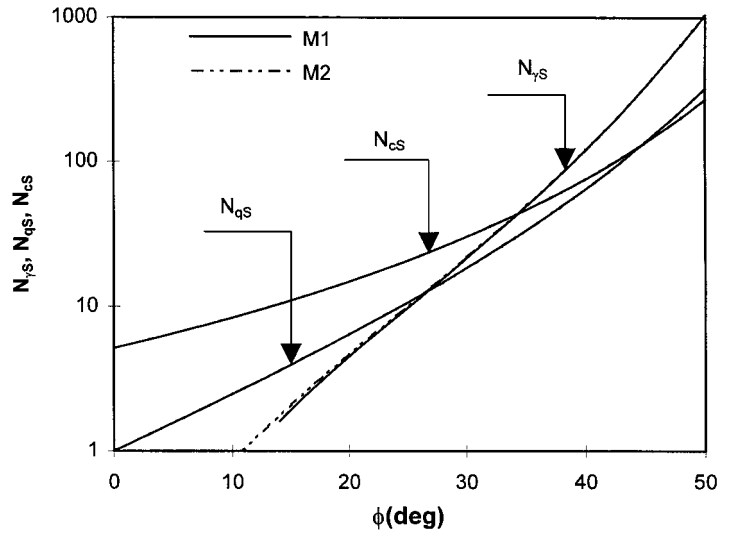


FIG. 9. Comparison of Bearing Capacity Factors given by M1 and M2 Mechanisms

Comparison of Results with Solutions of M2 Mechanism

The $N_{\gamma s}$, N_{qs} , and N_{cs} factors given by the M2 nonsymmetrical mechanism for $K_h = 0$ are presented in Table 5 and compared to those given by the M1 mechanism in Fig. 9. While the N_{qs} and N_{cs} factors are practically identical in both mechanisms, the M2 mechanism gives greater upper-bound solutions than the M1 mechanism for the $N_{\gamma s}$ factor. Notice, however, that the maximal difference does not exceed 4% for $\phi \geq 20^\circ$.

Seismic Bearing Capacity Factors

Earthquakes have the unfavorable effect of decreasing the bearing capacity of foundations. To investigate how the bearing capacity factors $N_{\gamma E}$, N_{qE} , and N_{cE} are affected, extensive numerical results based on the M2 failure mechanism are presented in Tables 6–8. All results are given for $n = 14$, which means that the minimization procedure is made with regard to 28 angular parameters.

Fig. 10 shows the critical slip surfaces obtained from the numerical minimization of the $N_{\gamma E}$ factor for $\phi = 30^\circ$ and for three values of K_h ($K_h = 0, 0.15$, and 0.3). It can be observed that the critical slip surface becomes shallower as the acceleration intensity increases.

Charts relating bearing capacity factors $N_{\gamma E}$, N_{qE} , and N_{cE} to various governing parameters are presented in Figs. 11–13.

TABLE 6. Seismic Bearing Capacity Factor $N_{\gamma E}$

K_h (1)	ϕ						
	15 (2)	20 (3)	25 (4)	30 (5)	35 (6)	40 (7)	45 (8)
0	2.10	4.67	10.06	21.88	49.62	120.96	328.88
0.05	1.51	3.57	7.91	17.43	39.69	96.48	259.93
0.1	1.01	2.61	6.04	13.59	31.23	75.92	203.11
0.15	0.58	1.80	4.45	10.35	24.14	58.94	156.98
0.2	0.26	1.13	3.14	7.67	18.32	45.12	120.05
0.25	0.04	0.62	2.09	5.51	13.61	34.05	90.85
0.3	—	0.26	1.28	3.80	9.89	25.31	68.05
0.35	—	—	0.69	2.49	6.99	18.51	50.44
0.4	—	—	0.28	1.51	4.77	13.29	36.99
0.45	—	—	0.04	0.81	3.12	9.34	26.82
0.5	—	—	—	0.35	1.92	6.40	19.19
0.55	—	—	—	0.07	1.08	4.24	13.54
0.6	—	—	—	—	0.51	2.69	9.38

TABLE 7. Seismic Bearing Capacity Factor N_{qE}

K_h (1)	ϕ						
	15 (2)	20 (3)	25 (4)	30 (5)	35 (6)	40 (7)	45 (8)
0	3.95	6.41	10.69	18.46	33.43	64.55	135.91
0.05	3.52	5.72	9.51	16.35	29.44	56.39	117.46
0.1	3.07	5.02	8.35	14.34	25.70	48.89	100.85
0.15	2.59	4.32	7.24	12.44	22.25	42.08	86.05
0.2	2.07	3.62	6.17	10.67	19.08	35.96	73.00
0.25	1.46	2.94	5.17	9.04	16.22	30.52	61.60
0.3	—	2.25	4.22	7.54	13.65	25.73	51.71
0.35	—	1.46	3.33	6.19	11.37	21.53	43.21
0.4	—	—	2.47	4.97	9.36	17.89	35.93
0.45	—	—	1.56	3.86	7.59	14.74	29.75
0.5	—	—	—	2.85	6.04	12.04	24.51
0.55	—	—	—	1.86	4.69	9.72	20.09
0.6	—	—	—	—	3.49	7.75	16.36

TABLE 8. Seismic Bearing Capacity Factor N_{cE}

K_h (1)	ϕ						
	15 (2)	20 (3)	25 (4)	30 (5)	35 (6)	40 (7)	45 (8)
0	11.00	14.87	20.78	30.25	46.35	75.80	135.09
0.05	10.26	13.79	19.14	27.64	41.95	67.84	119.27
0.1	9.50	12.69	17.50	25.09	37.74	60.38	104.74
0.15	8.72	11.60	15.91	22.64	33.76	53.46	91.56
0.2	7.96	10.54	14.37	20.32	30.06	47.12	79.70
0.25	7.21	9.51	12.91	18.14	26.63	41.36	69.14
0.3	6.48	8.53	11.53	16.12	23.50	36.18	59.81
0.35	5.79	7.61	10.25	14.26	20.67	31.56	51.62
0.4	5.14	6.75	9.07	12.58	18.12	27.47	44.49
0.45	4.54	5.96	8.00	11.05	15.85	23.86	38.29
0.5	3.98	5.23	7.02	9.68	13.83	20.69	32.94
0.55	3.47	4.58	6.14	8.46	12.04	17.93	28.33
0.6	3.01	3.98	5.36	7.37	10.48	15.53	24.37

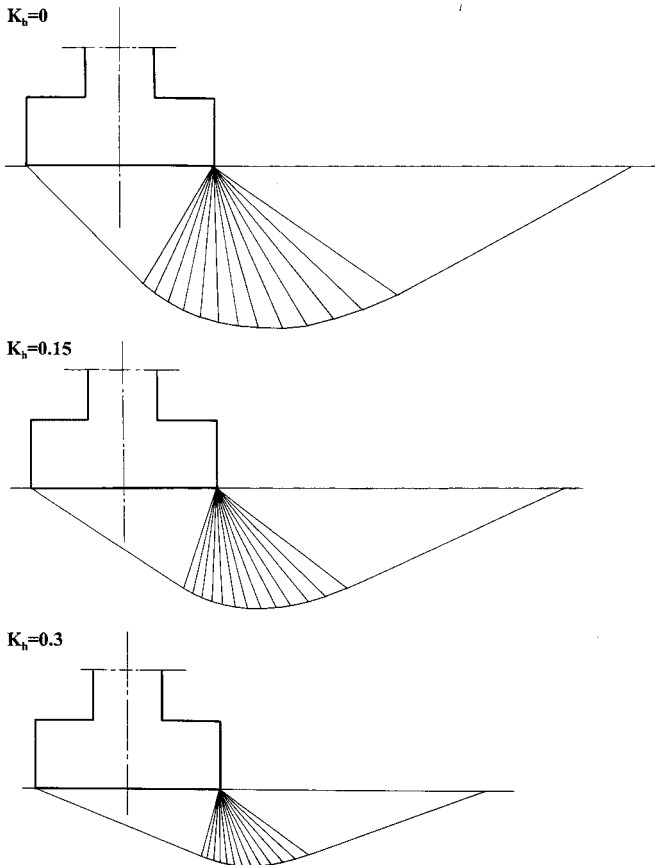


FIG. 10. Critical Slip Surfaces for $\phi = 30^\circ$ and $K_h = 0, 0.15,$ and 0.3

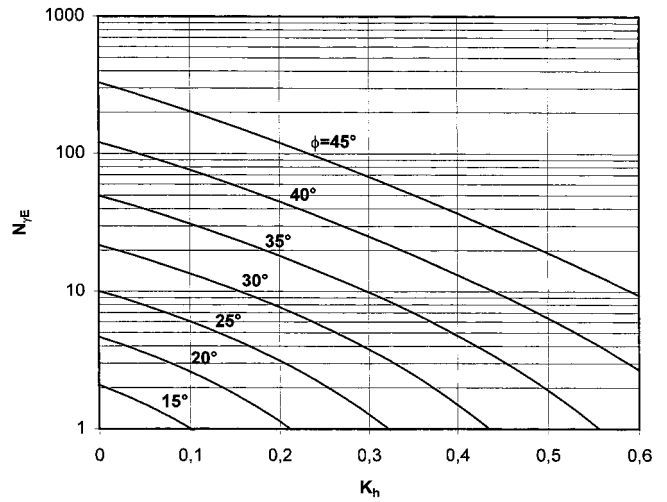


FIG. 11. Design Chart for N_{qE}

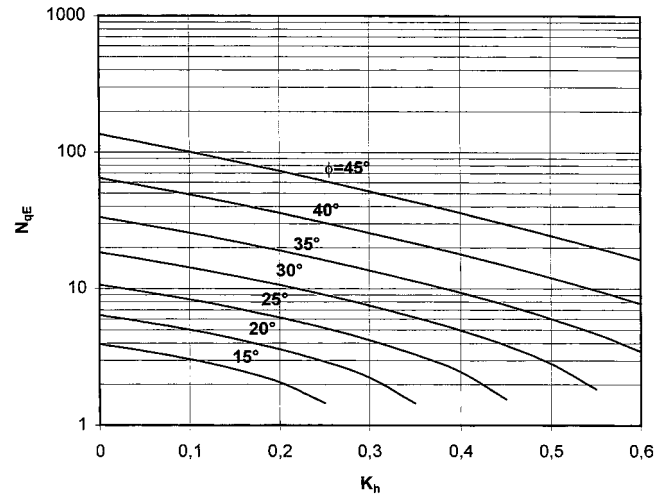


FIG. 12. Design Chart for N_{cE}

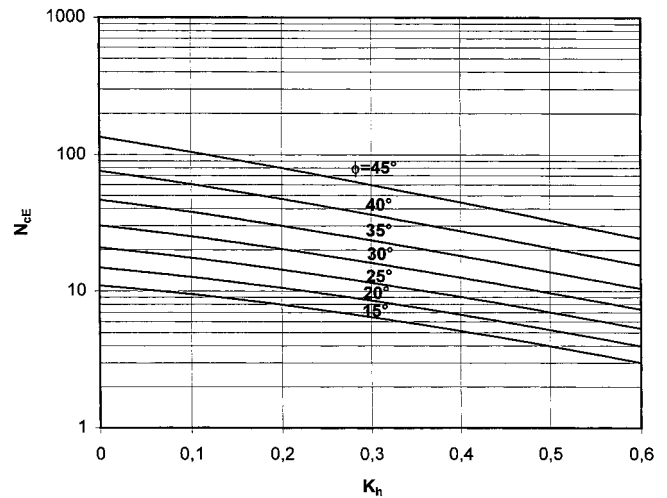


FIG. 13. Design Chart for N_{cE}

Comparison of Results with Existing Solutions

To see the validity of the present upper-bound solution, the seismic bearing capacity factors are calculated and compared with other solutions. The differences between them are discussed.

Soubra (1997) considered two nonsymmetrical failure mechanisms and gave rigorous upper-bound solutions in the framework of the limit analysis theory. One mechanism is

TABLE 9. Comparison of Present Seismic Bearing Capacity Factors with Upper-Bound Solutions Given by Soubra (1997) for $\phi = 40^\circ$

K_h (1)	$N_{\gamma E}$		N_{qE}		N_{cE}	
	Present solution (2)	Soubra (1997) (3)	Present solution (4)	Soubra (1997) (5)	Present solution (6)	Soubra (1997) (7)
0	121.0	140.5	64.6	64.2	75.8	75.3
0.1	75.9	88.4	48.9	48.7	60.4	60.1
0.2	45.1	53.0	36.0	35.9	47.1	46.9
0.3	25.3	30.1	25.7	25.7	36.2	36.1
0.4	13.3	16.0	17.9	17.9	27.5	27.4
0.5	6.4	7.8	12.0	12.0	20.7	20.7
0.6	2.7	3.3	7.8	7.7	15.5	15.5

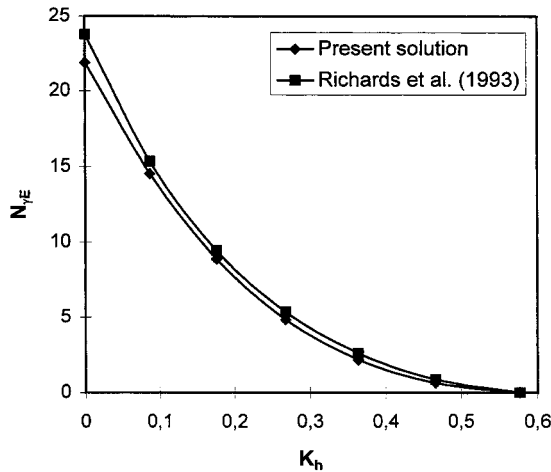


FIG. 14. Comparison of Present $N_{\gamma E}$ Factor with that of Richards et al. (1993) for $\phi = 30^\circ$

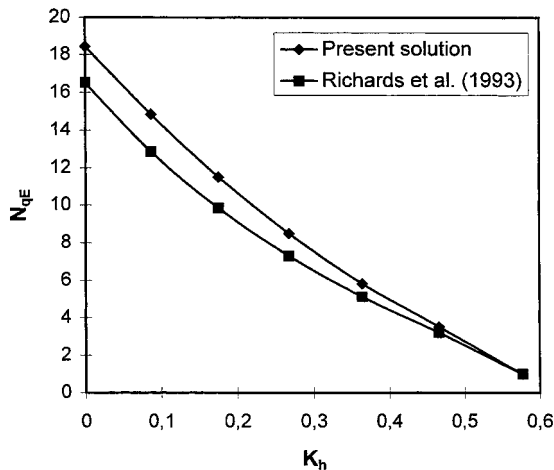


FIG. 15. Comparison of Present N_{qE} Factor with that of Richards et al. (1993) for $\phi = 30^\circ$

composed of a triangular active wedge under the footing, one radial log-spiral shear zone, and one triangular passive wedge. The other closely resembles the previous mechanism; however, the shear zone is now bounded by a circular arc. In the spirit of the upper-bound approach, the lesser of these two solutions was given in the form of design charts [cf. Soubra (1997)]. The upper-bound solutions given by the present M2 mechanism and those given by Soubra (1997) are presented in Table 9. It is clear that the present upper-bound solutions are better than those of Soubra (1997) for the $N_{\gamma E}$ factor; the improvement exceeds 15% for $K_h = 0.3$. However, the N_{qE} and N_{cE} factors are practically identical.

On the other hand, Figs. 14–16 show the comparison be-

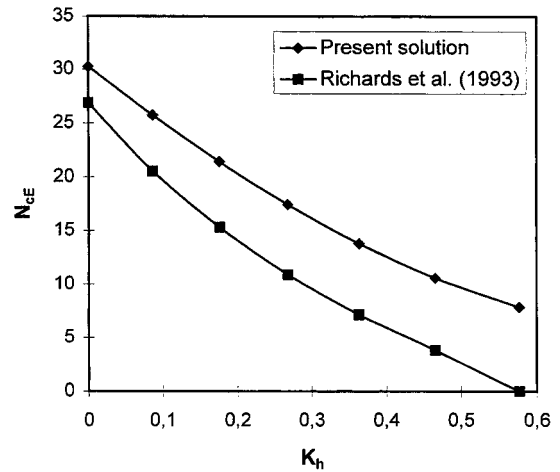


FIG. 16. Comparison of Present N_{cE} Factor with that of Richards et al. (1993) for $\phi = 30^\circ$

tween the present results and those given by Richards et al. (1993). From Fig. 14, it can be observed that the solutions given by Richards et al. (1993) slightly overestimate the $N_{\gamma E}$ factor with regard to the present upper-bound solutions. Concerning the N_{qE} factor (cf. Fig. 15), the maximal difference with Richards et al. (1993) does not exceed 14%. However, for the N_{cE} factor (cf. Fig. 16), the difference is equal to 11% for $\phi = 30^\circ$ and $K_h = 0$ and attains 40% for $K_h = 0.3$. This difference may be explained by the fact that Richards et al. (1993) have used (15) to calculate the seismic factor N_{cE} without any real justification as they mentioned in their paper.

CONCLUSIONS

Two failure mechanisms have been considered for the analysis of the static and seismic bearing capacity factors using the upper-bound method of the limit analysis theory. The solutions presented are rigorous upper-bound ones in the framework of the limit analysis theory. The numerical results obtained lead to the following conclusions.

For the static case, both the M1 symmetrical and the M2 nonsymmetrical mechanisms give the exact solution of the static N_{qS} and N_{cS} factors. For the $N_{\gamma S}$ factor, the M2 mechanism gives greater upper-bound solutions than the M1 mechanism. Notice, however, that the maximal difference does not exceed 4% for $\phi \geq 20^\circ$. The present upper-bound solutions are better than those of Chen (1975) since one obtains smaller upper-bound solutions; the improvement attains 15% for $\phi = 40^\circ$. On the other hand, the comparison between the present solutions and the currently accepted values of Caquot and Kérisel has shown that the maximal difference between the results is smaller than 10% for $\phi \leq 45^\circ$.

For the seismic case, the present upper-bound solutions given by the M2 nonsymmetrical mechanism are better than those of Soubra (1997) for the $N_{\gamma E}$ factor, the improvement exceeds 15% when $\phi = 40^\circ$ and $K_h = 0.3$. However, the N_{qE} and N_{cE} factors are practically identical to those given by Soubra (1997). On the other hand, the comparison with the solutions given by Richards et al. (1993) using the limit-equilibrium method has shown that the present upper-bound solutions are in agreement with regard to the results of Richards et al. for the $N_{\gamma E}$ and N_{qE} factors. However, for the N_{cE} factor, the difference between the present solution and that of Richards et al. attains 40% for $\phi = 30^\circ$ and $K_h = 0.3$. The present numerical results are presented in the form of design charts for practical use in geotechnical engineering.

APPENDIX I. M1 Mechanism

In this appendix, we present the different expressions for the incremental external work of mechanism M1, together with the internal energy dissipation from the same mechanism.

Geometry

For the triangular block i , the lengths l_i and d_i , and the surface S_i are given as follows:

$$l_i = \frac{B_0}{2 \cos \theta} \prod_{j=1}^{i-1} \frac{\sin \beta_j}{\sin(\alpha_j + \beta_j)} \quad (16)$$

$$d_i = \frac{B_0}{2 \cos \theta} \frac{\sin \alpha_i}{\sin(\alpha_i + \beta_i)} \prod_{j=1}^{i-1} \frac{\sin \beta_j}{\sin(\alpha_j + \beta_j)} \quad (17)$$

$$S_i = \frac{B_0^2}{2} \frac{\sin \alpha_i \sin \beta_i}{4 \cos^2 \theta \sin(\alpha_i + \beta_i)} \prod_{j=1}^{i-1} \frac{\sin^2 \beta_j}{\sin^2(\alpha_j + \beta_j)} \quad (18)$$

Incremental External Work

The different elements of the incremental external work for the M1 mechanism can be calculated as follows.

1. Incremental external work due to self-weight of triangle ABC_1

$$\Delta W_{ABC_1} = \frac{\gamma B_0^2}{2} [f_1(\alpha_i, \beta_i, \theta)] V_0 \quad (19)$$

where

$$f_1 = \frac{\tan \theta}{2} \quad (20)$$

2. Incremental external work due to self-weights of the remaining $2n$ triangular blocks

$$\sum_{j=1}^{2n} [\Delta W]_j = \frac{\gamma B_0^2}{2} [f_2(\alpha_i, \beta_i, \theta)] V_0 \quad (21)$$

where

$$f_2 = \frac{\cos(\theta - \phi)}{2 \cos^2 \theta \sin(\beta_1 - 2\phi)} \cdot \sum_{i=1}^n \left[\frac{\sin \alpha_i \sin \beta_i}{\sin(\alpha_i + \beta_i)} \sin \left(\beta_i - \theta - \sum_{j=1}^{i-1} \alpha_j - \phi \right) \cdot \prod_{j=1}^{i-1} \frac{\sin^2 \beta_j \sin(\alpha_j + \beta_j - 2\phi)}{\sin^2(\alpha_j + \beta_j) \sin(\beta_{j+1} - 2\phi)} \right] \quad (22)$$

3. Incremental external work due to the foundation load

$$\Delta W_{P_s} = P_s V_0 \quad (23)$$

4. Incremental external work due to the surcharge loading

$$\Delta W_q = q B_0 f_3(\alpha_i, \beta_i, \theta) V_0 \quad (24)$$

where

$$f_3 = \frac{\cos(\theta - \phi)}{\cos \theta \sin(\beta_1 - 2\phi)} \frac{\sin \beta_n}{\sin(\alpha_n + \beta_n)} \sin \left(\beta_n - \theta - \sum_{j=1}^{n-1} \alpha_j - \phi \right) \cdot \prod_{j=1}^{n-1} \frac{\sin \beta_j \sin(\alpha_j + \beta_j - 2\phi)}{\sin(\alpha_j + \beta_j) \sin(\beta_{j+1} - 2\phi)} \quad (25)$$

The total incremental external work is the summation of these four contributions, that is, (19), (21), (23), and (24)

$$\sum [\Delta W]_{\text{ext}} = \Delta W_{ABC_1} + \sum_{j=1}^{2n} [\Delta W]_j + \Delta W_{P_s} + \Delta W_q \quad (26)$$

Incremental Internal Energy Dissipation

1. Along BC

$$\Delta D_{BC} = c B_0 f_4(\alpha_i, \beta_i, \theta) V_0 \quad (27)$$

where

$$f_4 = \frac{\cos \phi \cos(\beta_1 - \theta - \phi)}{2 \cos \theta \sin(\beta_1 - 2\phi)} \quad (28)$$

2. Along lines d_i ($i = 1, \dots, n$)

$$\Delta D_{d_i(i=1, \dots, n)} = c B_0 f_5(\alpha_i, \beta_i, \theta) V_0 \quad (29)$$

where

$$f_5 = \frac{\cos(\theta - \phi) \cos \phi}{2 \cos \theta \sin(\beta_1 - 2\phi)} \cdot \sum_{i=1}^n \left[\frac{\sin \alpha_i}{\sin(\alpha_i + \beta_i)} \prod_{j=1}^{i-1} \frac{\sin \beta_j \sin(\alpha_j + \beta_j - 2\phi)}{\sin(\alpha_j + \beta_j) \sin(\beta_{j+1} - 2\phi)} \right] \quad (30)$$

3. Along the radial lines l_i ($i = 2, \dots, n$)

$$\Delta D_{l_i(i=2, \dots, n)} = c B_0 f_6(\alpha_i, \beta_i, \theta) V_0 \quad (31)$$

where

$$f_6 = \frac{\cos(\theta - \phi) \cos \phi}{2 \cos \theta \sin(\beta_1 - 2\phi)} \cdot \sum_{i=2}^n \left[\frac{\sin(\beta_{i-1} - \beta_i + \alpha_{i-1})}{\sin(\beta_i - 2\phi)} \prod_{j=1}^{i-1} \frac{\sin \beta_j}{\sin(\alpha_j + \beta_j)} \cdot \prod_{j=1}^{i-2} \frac{\sin(\alpha_j + \beta_j - 2\phi)}{\sin(\beta_{j+1} - 2\phi)} \right] \quad (32)$$

The total incremental energy dissipation is twice the summation of these three parts, that is, (27), (29), and (31)

$$\sum [\Delta D] = 2(\Delta D_{BC} + \Delta D_{d_i(i=1, \dots, n)} + \Delta D_{l_i(i=2, \dots, n)}) \quad (33)$$

APPENDIX II. M2 Mechanism

In this appendix, we present the different expressions for the incremental external work of mechanism M2, together with the internal energy dissipation for the same mechanism.

Geometry

For the triangular block i , the lengths l_i and d_i , and the surface S_i are given as follows:

$$l_i = B_0 \frac{\sin \beta_1}{\sin(\alpha_1 + \beta_1)} \prod_{j=2}^i \frac{\sin \beta_j}{\sin(\alpha_j + \beta_j)} \quad (34)$$

$$d_i = B_0 \frac{\sin \beta_1}{\sin(\alpha_1 + \beta_1)} \frac{\sin \alpha_i}{\sin \beta_i} \prod_{j=2}^i \frac{\sin \beta_j}{\sin(\alpha_j + \beta_j)} \quad (35)$$

$$S_i = \frac{B_0^2}{2} \frac{\sin^2 \beta_1}{\sin^2(\alpha_1 + \beta_1)} \frac{\sin \alpha_i \sin(\alpha_i + \beta_i)}{\sin \beta_i} \prod_{j=2}^i \frac{\sin^2 \beta_j}{\sin^2(\alpha_j + \beta_j)} \quad (36)$$

Incremental External Work

The different elements of the incremental external work for the M2 mechanism can be calculated as follows.

1. Incremental external work due to self-weights and inertia forces of the n triangular rigid blocks

$$\Delta W_{\text{soil}} = \frac{\gamma B_0^2}{2} [g_1(\alpha_i, \beta_i) + K_n g_2(\alpha_i, \beta_i)] V_1 \quad (37)$$

where

$$g_1 = \frac{\sin^2 \beta_1}{\sin^2(\alpha_1 + \beta_1)} \sum_{i=1}^n \left[\frac{\sin \alpha_i \sin(\alpha_i + \beta_i)}{\sin \beta_i} \sin \left(\beta_i - \phi - \sum_{j=1}^{i-1} \alpha_j \right) \cdot \prod_{j=2}^i \frac{\sin^2 \beta_j}{\sin^2(\alpha_j + \beta_j)} \prod_{j=1}^{i-1} \frac{\sin(\alpha_j + \beta_j - 2\phi)}{\sin(\beta_{j+1} - 2\phi)} \right] \quad (38)$$

$$g_2 = \frac{\sin^2 \beta_1}{\sin^2(\alpha_1 + \beta_1)} \sum_{i=1}^n \left[\frac{\sin \alpha_i \sin(\alpha_i + \beta_i)}{\sin \beta_i} \cos \left(\beta_i - \phi - \sum_{j=1}^{i-1} \alpha_j \right) \cdot \prod_{j=2}^i \frac{\sin^2 \beta_j}{\sin^2(\alpha_j + \beta_j)} \prod_{j=1}^{i-1} \frac{\sin(\alpha_j + \beta_j - 2\phi)}{\sin(\beta_{j+1} - 2\phi)} \right] \quad (39)$$

2. Incremental external work due to the foundation load and the corresponding inertia force

$$\Delta W_{P_E} = P_E [\sin(\beta_1 - \phi) + K_n \cos(\beta_1 - \phi)] V_1 \quad (40)$$

3. Incremental external work due to the surcharge loading and the corresponding inertia force

$$\Delta W_q = q B_0 [g_3(\alpha_i, \beta_i) + K_h g_4(\alpha_i, \beta_i)] V_1 \quad (41)$$

where

$$g_3 = \frac{\sin \beta_1}{\sin(\alpha_1 + \beta_1)} \sin \left(\beta_n - \phi - \sum_{j=1}^{n-1} \alpha_j \right) \cdot \prod_{j=2}^n \frac{\sin \beta_j}{\sin(\alpha_j + \beta_j)} \prod_{j=1}^{n-1} \frac{\sin(\alpha_j + \beta_j - 2\phi)}{\sin(\beta_{j+1} - 2\phi)} \quad (42)$$

$$g_4 = \frac{\sin \beta_1}{\sin(\alpha_1 + \beta_1)} \cos \left(\beta_n - \phi - \sum_{j=1}^{n-1} \alpha_j \right) \cdot \prod_{j=2}^n \frac{\sin \beta_j}{\sin(\alpha_j + \beta_j)} \prod_{j=1}^{n-1} \frac{\sin(\alpha_j + \beta_j - 2\phi)}{\sin(\beta_{j+1} - 2\phi)} \quad (43)$$

The total incremental external work is the summation of these contributions, that is, (37), (40), and (41)

$$\sum [\Delta W]_{\text{ext}} = \Delta W_{\text{soil}} + \Delta W_{P_E} + \Delta W_q \quad (44)$$

Incremental Internal Energy Dissipation

1. Along lines d_i ($i = 1, \dots, n$)

$$\Delta D_{d_i(i=1, \dots, n)} = c B_0 g_5(\alpha_i, \beta_i) V_1 \quad (45)$$

where

$$g_5 = \frac{\sin \beta_1 \cos \phi}{\sin(\alpha_1 + \beta_1)} \sum_{i=1}^n \left[\frac{\sin \alpha_i}{\sin \beta_i} \prod_{j=2}^i \frac{\sin \beta_j}{\sin(\alpha_j + \beta_j)} \cdot \prod_{j=1}^{i-1} \frac{\sin(\alpha_j + \beta_j - 2\phi)}{\sin(\beta_{j+1} - 2\phi)} \right] \quad (46)$$

2. Along the radial lines l_i ($i = 1, \dots, n - 1$)

$$\Delta D_{l_i(i=1, \dots, n-1)} = c B_0 g_6(\alpha_i, \beta_i) V_1 \quad (47)$$

where

$$g_6 = \frac{\sin \beta_1 \cos \phi}{\sin(\alpha_1 + \beta_1)} \sum_{i=1}^{n-1} \left[\frac{\sin(\beta_i - \beta_{i+1} + \alpha_i)}{\sin(\beta_{i+1} - 2\phi)} \prod_{j=2}^i \frac{\sin \beta_j}{\sin(\alpha_j + \beta_j)} \cdot \prod_{j=1}^{i-1} \frac{\sin(\alpha_j + \beta_j - 2\phi)}{\sin(\beta_{j+1} - 2\phi)} \right] \quad (48)$$

The total incremental energy dissipation is the summation of these two parts, that is, (45) and (47)

$$\sum [\Delta D] = \Delta D_{d_i(i=1, \dots, n)} + \Delta D_{l_i(i=1, \dots, n-1)} \quad (49)$$

APPENDIX III. REFERENCES

Caquot, A., and Kérisel, J. (1953). "Sur le terme de surface dans le calcul des fondations en milieu pulvérulent." *Proc., 3rd Int. Conf. on Soil Mech. and Found. Engrg.*, ICOSOMES, Zurich, Vol. I, 336–337.

Chen, W. F. (1975). *Limit analysis and soil plasticity*. Elsevier Scientific Publishing Company, London, 637.

Davis, E. H. (1968). "Theories of plasticity and the failure of soil masses." *Soil mechanics: Selected topics*, I. K. Lee, ed., Butterworth's, London, 341–380.

De Buhan, P., and Salençon, J. (1993). "A comprehensive stability analysis of soil nailed structures." *Eur. J. Mech. Ser. A/Solids*, Paris, 12(3), 325–345.

Dormieux, L., and Pecker, A. (1995). "Seismic bearing capacity of foundations on cohesionless soil." *J. Geotech. Engrg.*, ASCE, 121(3), 300–303.

Drescher, A., and Detournay, E. (1993). "Limit load in translational failure mechanisms for associative and non-associative materials." *Géotechnique*, The Institution of Civil Engineers, London, 43(3), 443–456.

Meyerhof, G. G. (1951). "The ultimate bearing capacity of foundations." *Géotechnique*, The Institution of Civil Engineers, London, 2, 301–332.

Meyerhof, G. G. (1963). "Some recent research on the bearing capacity of foundations." *Can. Geotech. J.*, Ottawa, 1(1), 16–26.

Michalowski, R. L. (1989). "Three-dimensional analysis of locally loaded slopes." *Géotechnique*, The Institution of Civil Engineers, London, 39(1), 27–38.

Michalowski, R. L., and Shi, L. (1995). "Bearing capacity of footings over two-layer foundation soils." *J. Geotech. Engrg.*, ASCE, 121(5), 421–428.

Michalowski, R. L., and Shi, L. (1996). "Closure on 'Bearing capacity of footings over two-layer foundation soils.'" *J. Geotech. Engrg.*, 122(8), 701–703.

Mroz, Z., and Drescher, A. (1969). "Limit plasticity approach to some cases of flow of bulk solids." *J. Engrg. Ind. Trans.*, ASCE, 91, 357–364.

Richards, R., Elms, D. G., and Budhu, M. (1993). "Seismic bearing capacity and settlement of foundations." *J. Geotech. Engrg.*, ASCE, 119(4), 662–674.

Salençon, J. (1990). "An introduction to the yield design theory and its application to soil mechanics." *Eur. J. Mech. Ser. A/Solids*, Paris, 9(5), 477–500.

Sarma, S. K., and Iossifelis, I. S. (1990). "Seismic bearing capacity factors of shallow strip footings." *Géotechnique*, The Institution of Civil Engineers, London, 40(2), 265–273.

Shinohara, T., Tateishi, T., and Kubo, K. (1960). "Bearing capacity of sandy soil for eccentric and inclined load and lateral resistance of single piles embedded in sandy soil." *Proc., 2nd World Conf. on Earthquake Engrg.*, Tokyo, Gabujutsu bunken sukuyu-rai, Vol. 1, 265–280.

Soubra, A.-H. (1997). "Seismic bearing capacity of shallow strip footings in seismic conditions." *Proc., Instn. Civ. Engrs., Geotech. Engrg.*, London, 125(4), 230–241.

Terzaghi, K. (1943). *Theoretical soil mechanics*. Wiley, New York, 510.

Vesic, A. S. (1973). "Analysis of ultimate loads of shallow foundations." *Proc., ASCE*, 99(1), 45–73.

APPENDIX IV. NOTATION

The following symbols are used in this paper:

- B_0 = width of footing;
- c = cohesion;
- c^* = residual cohesion due to nonassociativeness;
- d_i, l_i = discontinuity lines;
- K_h = horizontal seismic coefficient;
- $N_{\gamma E}, N_{q E}, N_{c E}$ = seismic bearing capacity factors;
- $N_{\gamma S}, N_{q S}, N_{c S}$ = static bearing capacity factors;
- n = number of rigid blocks in failure mechanisms;
- P_E = seismic ultimate load;
- P_S = static ultimate load;
- q = surcharge loading;
- $q_{c E}$ = seismic bearing capacity of footing;
- $q_{c S}$ = static bearing capacity of footing;
- S_i = area of block i ;
- V_0 = initial downward velocity of footing for M1 mechanism;
- V_1, V_2, \dots, V_n = velocities of blocks 1, 2, \dots , n ;
- γ = unit weight of soil;
- ΔV = velocity along velocity discontinuity;
- $\theta, \alpha_i, \beta_i$ = angular parameters of failure mechanisms;
- ϕ = angle of internal friction of soil;
- ϕ^* = residual friction angle due to nonassociativeness; and
- Ψ = dilatancy angle.